Electron-doped organics: Charge-disproportionate insulators and Hubbard-Fröhlich metals

note finali coverpage

(Article begins on next page)

06 May 2024

Electron doped organics: charge-disproportionate insulators and Hubbard-Fröhlich metals

S. Shahab Naghavi,[1] Michele Fabrizio,[1] Tao Qin,[1] and Erio Tosatti[1,2]

[1]*International School for Advanced Studies (SISSA),*
and CNR-IOM Democritos National Simulation Center, Via Bonomea 265, I-34136 Trieste, Italy
[2]*International Centre for Theoretical Physics (ICTP), Strada Costiera 11, I-34151 Trieste, Italy*
(Dated: September 24, 2018)

Several examples of metallic electron doped polycyclic aromatic hydrocarbons (PAHs) molecular crystals have recently been experimentally proposed. Some of them have superconducting components, but most other details are still unknown beginning with structure and the nature of metallicity. We carried out *ab-initio* density functional calculations for La-Phenanthrene (La-PA), here meant to represent a generic case of three-electron doping, to investigate structure and properties of a conceptually simple case. To our surprise we found first of all that the lowest energy state is not metallic but band insulating, with a disproportionation of two inequivalent PA molecular ions and a low $P1$ symmetry, questioning the common assumption that three electrons will automatically metallize a PAH crystal. Our best metallic structure is metastable and slightly higher in energy, and retains equivalent PA ions and a higher $P2_1$ symmetry – the same generally claimed for metallic PAHs. We show that a "dimerizing" periodic distortion opens very effectively a gap in place of a symmetry related degeneracy of all $P2_1$ structures near the Fermi level, foreshadowing a possible role of that special intermolecular phonon in superconductivity of metallic PAHs. A Hubbard-Fröhlich model describing that situation is formulated for future studies.

PACS numbers: 74.70.Kn,71.15.Mb,71.10.Fd,71.20.Tx

I. INTRODUCTION

There is a continuing and expanding interest in the transformation, via electron doping, of insulating organic molecular crystals to molecular metals and especially to superconductors. Polycyclic aromatic hydrocarbons (PAHs) are a well known family of molecular crystals where intercalation of electron-donating atomic species recently rekindled attention in that direction. Pioneering reports include metallization with superconductivity in electron doped picene,[1] coronene,[2,3] dibenzopentacene, where T_c exceeds $30\,\text{K}$,[4] and phenanthrene.[5–7] To this date, many of these exciting systems are proving difficult to reproduce and characterize, and there remains considerable uncertainty across the board, ranging from precise stoichiometry, chemical composition, to crystal and electronic structure, the role of correlations, to superconductivity and its mechanism. Surface spectroscopies, intriguingly, generally fail even to show metallicity of the doped materials.[8,9] Early calculations[3,10–15] illustrated partial filling of LUMO+1 derived bands, weakly hybridized with higher energy alkali states. Electron-phonon calculations highlighted the coupling of these bands to intra-molecular but also inter-molecular lattice vibrations, potentially conducive to BCS superconductivity.[12] At the same time, large electron-electron repulsion parameters have been repeatedly emphasized,[11,13,16] suggesting possible analogies with alkali fullerides–molecular superconducting systems[17] earlier proposed[18] and recently shown[19,20] to be strongly correlated superconductors, close to a Mott-insulating state.[21] All that leaves the overall nature of doped PAHs, their insulating, metallic and superconducting phases, in a state of lamentable uncertainty.

Here we attempt a fresh theoretical start, based on accurate *ab-initio* total energy calculations and structural optimization of a particularly simple doped crystalline PAH system. As an alternative to previous studies, which also included a careful optimization of K-doped picene for various potassium concentrations,[13] we choose here the more speculative case of La-Phenanthrene (La-PA). With the single electropositive trivalent atom and the more compact PA molecule accepting or sharing three electrons, this is a conceptually and practically much simpler system. La-PA is reported to exist, and to superconduct near $6\,\text{K}$,[7] although this data has not been independently confirmed so far. In the context of a model theoretical study, hypothetical crystalline La-PA serves well as an idealized model system, sharing many of the properties of the wider class of electron doped PAHs, with reduced complexity. The PA molecule $C_{14}H_{10}$ is small and relatively rigid, and there is only one La cation to be located in the cell, next to it. This simplicity affords a much more intimate and exhaustive structural and electronic search. In turn, the results and modeling can be expected to fulfill a broader explorative scope, defining a prototype Hamiltonian of more general value, beyond the specific system chosen to define it.

In section II we describe density functional theory (DFT) calculations of total energy and electronic structure of La-PA as a function of all atomic coordinates in a bimolecular unit cell, with the scope of determining the nature of the lowest energy crystal structures and the corresponding electronic energy bands. Rather unexpectedly, we find that the optimal crystal structure is insulating due to a spontaneous disproportionation, where La

atom pairs preferentially bind to one PA molecule and less to the other. The spontaneous nonequivalence of the two PA molecules in the cell leads to a lower $P1$ lattice symmetry, directly leading to the opening of an insulating band gap. No such disproportionated state has so far emerged in previous theoretical studies of alkali doped PAHs, and in experimental studies; our results suggest that this possibility should be pursued. In our search for La-PA crystalline structures we also find at higher energy metallic structures with $P2_1$ symmetry, where the La cation is symmetrically equidistant among two PA anions. This high symmetry, similar to that proposed for many other postulated PAH superconductors, implies a symmetry-induced degeneracy near the Fermi level. We thus take it up this metallic phase and examine it as a simple prototype system, useful for the future development of further generic theoretical modeling of metallic electron doped PAHs, independently of whether a phase with these or nearby characteristics will actually be confirmed or not in La-PA. In section III, we downfold the electronic structure into a tight binding minimal two-band model on a basis of localized Wannier functions. In section IV, we briefly discuss how a frozen intermolecular phonon consisting of a simple dimerization of PA molecular pairs constitutes a gap-opening mode for electrons near Fermi, within the two LUMO+1 derived and partly degenerate bands. Reminiscent of the situation of MgB_2, the linear band splitting caused by a specific periodic distortion, foreshadows a strong role of a particular intermolecular phonon with PA-dimerizing eigenvector, in a hypothetical BCS type superconducting state. The third ingredient, already highlighted by previous studies, is the strong expected electron-electron repulsion within each molecular ion. As our final result we assemble the tight binding model and the electron phonon together with the intramolecular Coulomb interaction parameter U, thus forming what we designate a two-band *Hubbard-Fröhlich model*, which we consider a minimal model for future studies of this kind of potential superconductor. Finally, in section V we draw our conclusions.

II. DFT TOTAL ENERGY CALCULATIONS AND STRUCTURAL OPTIMIZATION OF LA-PA

Ab-initio electronic structure calculations for La-PA were carried out using the QUANTUM-ESPRESSO[22] code which implements the standard DFT framework within a plane waves basis set for one-electron wavefunctions. The Generalized Gradient Approximation (GGA) used a PBE exchange-correlation potential.[23] La was treated with Vanderbilt ultrasoft pseudopotentials,[24] whereas the potentials for carbon and oxygen, C.pbe-rrjkus.UPF and H.pbe-rrjkus.UPF, were taken from the QUANTUM-ESPRESSO web package. The k-point sampling for the integration in the Brillouin zone (BZ) yielded well converged results with $3\times4\times3$ Monkhorst-Pack k-point meshes. Plane wave cut-offs were 50 eV for

kinetic energy and 500 eV for charge density.

TABLE I. Theoretically DFT optimized structural parameters of the pristine phenanthrene molecular crystal, with $P2_1$ symmetry and two molecules per cell, obtained with different approximations, compared with experiment. Lengths in Angstrom units.

Source	a	b	c	α	β	γ	Vol.
Exp.[25]	8.46	6.16	9.47	90.0	97.7	90.0	489.1
GGA	9.25	6.31	9.71	90.0	100.6	90.0	557.4
vdW-DF[26]	8.51	6.19	9.49	90.0	98.2	90.0	494.8
vdW-DF2[27]	8.27	6.09	9.34	90.0	97.7	90.0	466.5
Grimme[28,29]	7.87	5.95	9.19	90.0	96.5	90.0	427.7

As a preliminary step we began with pristine phenanthrene (PA). As for all molecular crystals, we face the problem of van der Waals (vdW) forces, which dominate large distance intermolecular interactions but are missing in standard DFT, with uncontrolled errors in the optimal geometry and in the electronic structure. Aiming at a quantitative description of the pristine PA molecular crystal structure we tried different vdW schemes among those currently proposed. Assuming a bimolecular $P2_1$ symmetry unit cell as known experimentally, we found best agreement with the experimental structure parameters[25] of table I by complementing DFT with the vdW-DF functional.[26,30–32] All energy calculations in the rest of this paper were carried out including the vdW-DF contribution.

Thus equipped, we moved on to our main target, the electron-doped La-PA system. The experimental suggestion[7] that La-PA retains the same $P2_1$ symmetry of pristine PA was not forced; but we chose to restrict to the same minimal bimolecular unit cell. To explore within that bound the largest variety of structural configurations, we initially placed two PA molecules in the pristine crystal positions. A large number $n=114$ of empty spaces that could host a La atom between the PA molecules were identified using 76 and 31 pm respectively for the covalent radii of carbon and hydrogen, and 100–117 pm for the ionic radius of La^{+3}.[33] If two of these empty sites per cell are to be filled with La atoms, that can in principle be done in $\frac{n(n-1)}{2}= 6441$ different ways. Even though several configurations such as those with two La atoms closest to each other could be discarded as very unlikely, the overall number of La placements is still too large to be explored in full. We therefore adopted a shortcut strategy. First we started, as suggested by the experimental papers, with $P2_1$ symmetry of the two-molecule unit cell, see e.g. Fig. 1, thus spanning a much smaller set of structures, which we can explore in full. After that, random structures of lower ($P1$) symmetry were created by intermixing the position of La atoms taken from the few optimal high $P2_1$ symmetry structures. While of course this procedure is not equivalent to a full search, it does quite well as we shall see, bringing out unmistakeable novelties. In the restricted

$P2_1$ search, the first La is placed in n possible ways, and the second La position is completely determined by symmetry, reducing the number of starting geometries from $\frac{n(n-1)}{2}$ to $n=114$. The C_2 rotation axis moreover reduces that number by a further factor 2, down to $n/2$ = 57 different initial $P2_1$ trial structures. For each of them we calculated the DFT electronic structure, total energy, and forces acting on all atoms. The forces were then used for a relaxation of all atomic positions. A full optimization—lattice parameters as well as all internal coordinates—was performed for all structures. At convergence, residual forces acting on each atom were much smaller than $1\,\mathrm{mRy/a.u.}$. During the relaxation process, the La atoms sometimes moved by large amounts, so that different initial configurations often ended up to the same final, optimized structure. Therefore, at the end of optimization, all the 57 different structures were categorized to 18 different groups. The parameters for a few the lowest energy structures are given in table II and all are plotted in Fig. 2.
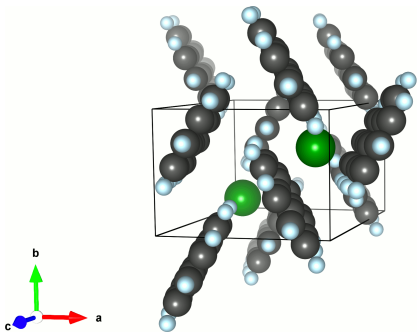

FIG. 1. (Color online) Schematic of one of 57 trial structures, with two PA molecules in the unit-cell, two La atoms (green) and $P2_1$ symmetry. These structures are subsequently relaxed, retaining at first a $P2_1$ symmetry. From the few best ones, additional trial structures of lower $P1$ symmetry are generated by exchanging La positions between them.

After this full $P2_1$ search, a set of random $P1$ trial structures were created by intermixing the position of La atoms of the best high symmetry $P2_1$ structures, as follows. If two $P2_1$ structures p and q have the two La atoms at positions $(\mathbf{P}, \mathbf{P}')$ and $(\mathbf{Q}, \mathbf{Q}')$ respectively, a new trial structure, generally of $P1$ symmetry, is created by placing the two La atoms at $(\mathbf{P}, \mathbf{Q})$, $(\mathbf{P}, \mathbf{Q}')$,$(\mathbf{Q}, \mathbf{P})$, etc. Additional sets of low symmetry trial structures were created by high temperature ab-initio molecular dynamics (MD) simulations[34] (see Table II). After that, newer attempts failed to yield radically new outcomes, and the variety of trial structures explored was deemed to be sufficient. DFT total energy and force calculation with subsequent optimization readily showed that several optimized $P1$ structures have a lower energy than the best $P2_1$ ones, thus confirming the correctness of exploring reduced symmetries. Parameters of the few lowest energy relaxed $P1$ structures are given in Table II. We note that they are close in energy and share a common feature: the

two La atoms in the cell approach the same PA molecule, rather than remaining equidistant between the two PA molecules as in the $P2_1$ structures. The two molecules display a slightly different shape, the isolated one now more planar than the other. An independent vibrational signature of this insulating phase could therefore consist of a characteristic splitting of the main intra-molecular vibrations reflecting the nonequivalence of the two PA molecules. Fig. 3, shows schematically the lowest $P1$ structures, labeled P1c. The second lowest $P1$ structure obtained by 8512 MD-steps (called 8512s in Table II) is nearly degenerate and isostructural with P1c. Indeed, as clear in Fig. 2, all attempts, i.e. MD simulations with different initial structures, end up to insulating phases with nearly similar structures and energy. Among the higher symmetry $P2_1$ structures, 18 and 36 are the lowest in energy, again nearly degenerate within our accuracy, and about 40 mRy per cell, that is more than 0.5 eV, higher than the $P1$ structures. The reason for this systematic energy lowering caused by disproportionation is best understood by careful consideration of the electronic structures, which we will do next.
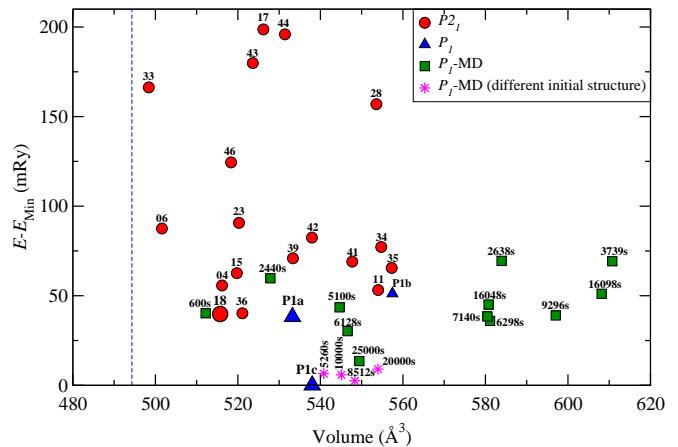

FIG. 2. (Color online) Energies and volumes per (bimolecular) cell for the main relaxed structures. The lowest energy structures of $P1$ symmetry are insulating, the metastable $P2_1$ structures are metallic. Magenta asterisks are MD-simulations starting from "P1a" structure rather than 18, shown by blue triangle. The dashed line shows the cell volume quoted in the experimental Ref. 7.

The electronic band structures of the optimized La-PA geometries are shown on Fig.4. All the $P2_1$ structures are metallic, owing to a symmetry-induced degeneracy within the LUMO+1 derived band (nearest to the Fermi level) on the zone boundary plane $k_y = \pm\pi$, see Fig. 4. This is a symmetry-induced degeneracy where bands "stick together" at zone boundary points, a well known property of "nonsymmorphic" space groups,[35] groups that include a mixed rotation-fractional translation symmetry operation. The $P2_1$ symmetry includes a screw axis along b, which makes the two PA molecules equivalent, while still distinct. The band degeneracy of $P2_1$

TABLE II. Energy and structural information of $P2_1$ structures and $P1$ structures of lowes energy. Lengths are in Angstrom and energies in mRy/bimolecular cell.

Samples	$E - E_{18}$[mRy]	a	b	c	α	β	γ	Volume
Exp.[7]	....	8.481	6.187	9.512	90.00	97.95	90.00	494.3
$P2_1 symmetry$								
18	0.0	8.55	6.61	10.07	90.00	115.11	90.00	515.70
36	0.4	8.62	6.59	9.93	90.00	112.46	90.00	521.10
11	13.4	8.54	7.24	9.01	90.00	96.01	90.00	554.01
4	15.9	8.37	6.63	9.49	90.00	101.14	90.00	516.17
$P1 symmetry$								
P1c	-39.8	9.73	5.83	9.73	86.12	101.89	93.26	538.01
8512s	-37.3	9.68	5.87	10.03	94.65	105.14	86.56	548.34
10000s	-34.0	9.75	5.80	10.56	91.78	113.92	86.41	545.08
5260s	-33.3	9.36	5.99	10.09	87.99	106.21	86.44	540.81
20000s	-30.9	9.80	5.87	10.57	91.95	114.05	86.64	553.95
25000s[a]	-26.3	9.08	6.95	10.99	92.93	127.21	83.52	549.44

[a] Initial structure of this MD simulation is 18, while for others is P1a

La-PA near the Fermi level bears similarities with that reported for the metallic state of other doped PAHs like K_3-picene.[10–14]. That invites a further pursuit of the present model $P2_1$ phase, even if only metastable in La-PA, as a generic model of metallic doped PAH possibly prone to superconductivity. This is what we will do later in the following sections.

The screw axis symmetry operation present in $P2_1$ is missing in the $P1$ structures, where the two LA molecules have become inequivalent. Because of that, the zone boundary degeneracy near $E_{\rm F}$ is lifted, and a band gap opens up which splits the two LUMO+1 derived bands leading to an insulating state. The $P1$ insulating state is thus closely connected with the valence disproportionation taking place at the structural level between the two PA molecules in the cell, one more closely approached, and partly covalently bonded, by the two La ions, the other more isolated. As seen in Fig.4 our calculated gap in La-PA is about 0.7 eV – probably an underestimate, as is generally the case in (self-interaction uncorrected) DFT. The striking parallelism of the valence and conduction bands further implies a strongly peaked joint density of states, suggesting large excitonic effects in optical absorbtion below the band gap.[36] We note that the present band insulating $P1$ state is a spin singlet, quite different from the antiferromagnetic band insulator state proposed for K_3-picene.[11] Starting with the best $P2_1$ structure 18 of La-PA, we also searched for magnetic solutions of our DFT calculations. While we could not stabilize a ferromagnetic state, we did find a locally stable antiferromagnetic state, where the two molecules remain equivalent in both structure and electronic charge, but exhibit oppositely polarized magnetizations of magnitude compatible with spin 1/2. However that solution was found for La-PA to lie only 0.7 mRy lower that the parent $P2_1$ non-magnetic metal, a minute energy gain by comparison with the ~40 mRy gain of the nonmagnetic insulating $P1$ structure.
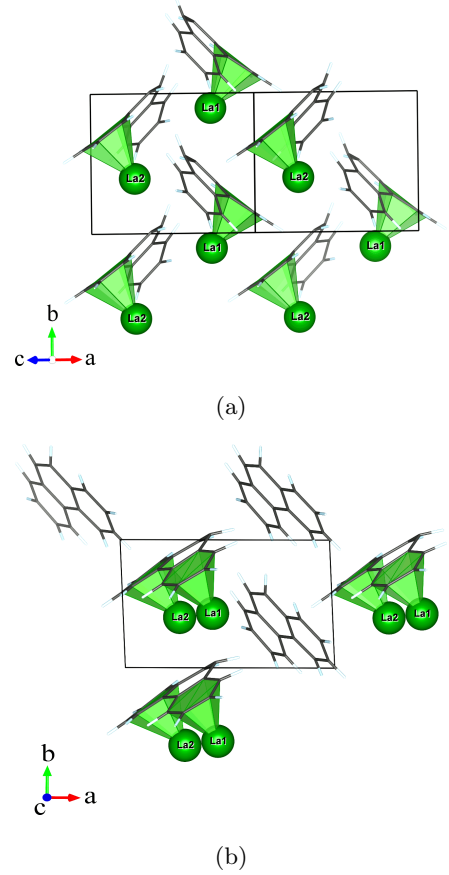

(a)

(b)

FIG. 3. (Color online) (a): Schematic of the best metallic structure 18 ($P2_1$ symmetry, metastable). The two PA molecules are equivalent, and heavily distorted, with La atoms positioned symmetrically between the two PA molecules. (b): Lowest energy insulating structure P1c ($P1$ symmetry, stable). Here the two molecules underwent a disproportionation, becoming spontaneously inequivalent, one preferentially bound to two La ions and less planar, the other more isolated and planar.
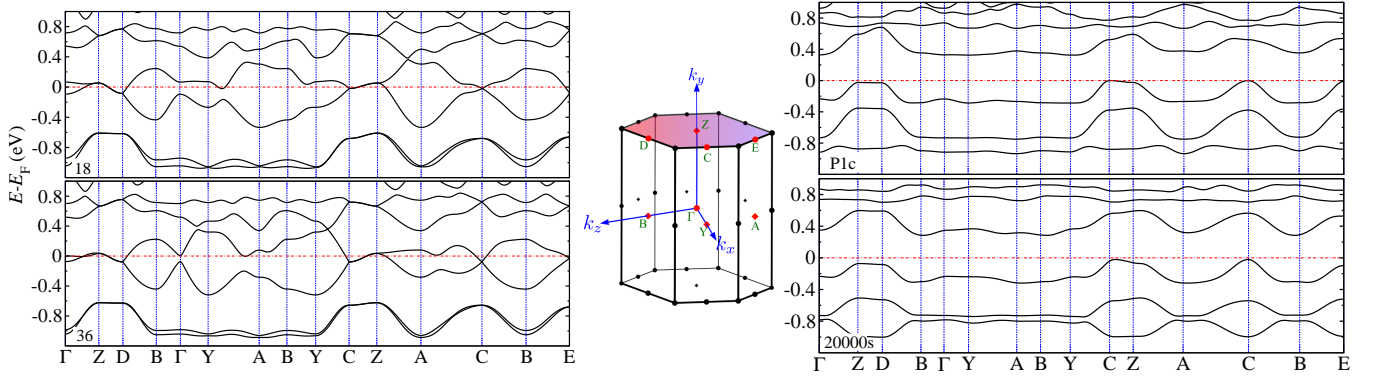
FIG. 4. (Color online) Electron band structures for the two best $P2_1$ structures 18 and 36, (metastable, metallic) and for the two best $P1$ structures P1c and 20000s (stable, insulating). The Brillouin Zone is also shown, highlighting the 010 boundary plane where symmetry induced band degeneracy occurs in the $P2_1$ structures.

Even if the $P2_1$ metallic structures are not of lowest energy, it is not unconceivable that they could still form and survive in a metastable state for kinetic reasons. In the rest of the paper we will concentrate on these metallic $P2_1$ phases, in particular on structure 18, as a possible, even if speculative, seat of superconductivity. Rather than addressing superconductivity at this stage, and notwithstanding the fact that some groups are currently pursuing electron-phonon coupling with direct *ab-initio* methods,[12,37] our alternative and present goal is to assemble in a single model what we believe could be the basic ingredients and elements for a simple scheme that would allow wider scope model superconductivity studies in the future. The elements we consider are of three kinds. The first is a minimal tight binding model electronic structure, including in this case only the two LUMO+1 derived bands. Similarly to earlier studies of K$_3$ picene,[11] we will do that for La-PA in the next section. As a second element we wish to identify at least one important lattice phonon that is strongly coupled to electrons near the Fermi level. We will argue in the subsequent section that symmetry suggests a "dimerizing" phonon, whose eigenvector instantaneously turns $P2_1$ symmetry to $P1$, as a natural candidate. The third element, widely discussed e.g., in Ref[11,13] is the electron-electron intra-molecular repulsion U. Good estimates are already available, for phenanthrene and other PAHs triply negative ions.[38] In the next two chapters we thus focus on modeling the tight binding bands and the main electron-phonon coupling.

III. TIGHT BINDING MODELING OF METALLIC BANDS

In order to extract the hopping parameter between Wannier functions centered on the two equivalent phenanthrene molecules "1" and "2" in the $P2_1$ cell, we implemented calculations using Wannier90[39] and fitted the two LUMO+1 derived metallic bands of structure 18

as highlighted by orange lines in Fig. 7 restricting only to hopping matrix elements $\gtrsim 0.01\,\mathrm{eV}$.

Fig. 5 (a) shows the *ab*-plane with the strongest hopping elements. Molecules "1" and "2" in the origin unit cell have coordinates $(0,0,0)$ and $\frac{1}{2}(1,1,0)$, respectively. We note that the molecular staggering brings about hopping amplitudes that are not invariant under $a \to -a$. The hopping matrix $\hat{t}_{\mathbf{k}}$ with elements $t_{\mathbf{k}}^{ij}$, $i,j = 1,2$ reads

$$\hat{t}_{\mathbf{k}} = \begin{pmatrix} t_{\mathbf{k}}^{11} & t_{\mathbf{k}}^{12} \\ t_{\mathbf{k}}^{21} & t_{\mathbf{k}}^{22} \end{pmatrix}, \tag{1}$$

where

$$t_{\mathbf{k}}^{12} = \left(1 + e^{-i\mathbf{k}\cdot\mathbf{b}}\right)\left(t_1 + t_2\,e^{-i\mathbf{k}\cdot\mathbf{a}} + t_3\,e^{i\mathbf{k}\cdot\mathbf{c}}\right) \equiv -e^{-i\theta_{\mathbf{k}}}\,\tau_{\mathbf{k}},$$

$t_{\mathbf{k}}^{21} = t_{\mathbf{k}}^{12\,*}$, and

$$\tau_{\mathbf{k}} = |\,t_{\mathbf{k}}^{12}\,| = 2\left|\cos\left(\frac{\mathbf{k}\cdot\mathbf{b}}{2}\right)\right|\left|t_1 + t_2\,e^{-i\mathbf{k}\cdot\mathbf{a}} + t_3\,e^{i\mathbf{k}\cdot\mathbf{c}}\right|, \tag{2}$$

while

$$t_{\mathbf{k}}^{11} = t_{\mathbf{k}}^{22} \equiv t_{\mathbf{k}} = 2t_4\cos\mathbf{k}\cdot\mathbf{b} + 2t_5\cos\mathbf{k}\cdot\mathbf{c} + 2t_6\cos\mathbf{k}\cdot(\mathbf{a}+\mathbf{c}).$$

The two bands have therefore a dispersion

$$\epsilon_{\pm\mathbf{k}} = t_{\mathbf{k}} \pm \tau_{\mathbf{k}}. \tag{3}$$

These model bands are degenerate on the whole plane $\mathbf{k}\cdot\mathbf{b} = \pi$, where in addition they disperse very little, see Fig. 4. The optimized hopping parameters are; $t_1 = -0.13$, $t_2 = 0.03$, $t_3 = 0.07$, $t_4 = -0.008$, $t_5 = 0.014$, $t_6 = 0.013$ (see Fig. 5).

We note that the degeneracy on the plane $\mathbf{k}\cdot\mathbf{b} = \pi$ can be easily lifted once the screw axis along b, a symmetry present in $P2_1$ structures, is removed. The removal can occur in different ways. The two molecules can cease to be equivalent as in the disproportionated $P1$ phase described above. Then $t_{\mathbf{k}}^{11} \neq t_{\mathbf{k}}^{22}$ in Eq. (1). In particular,
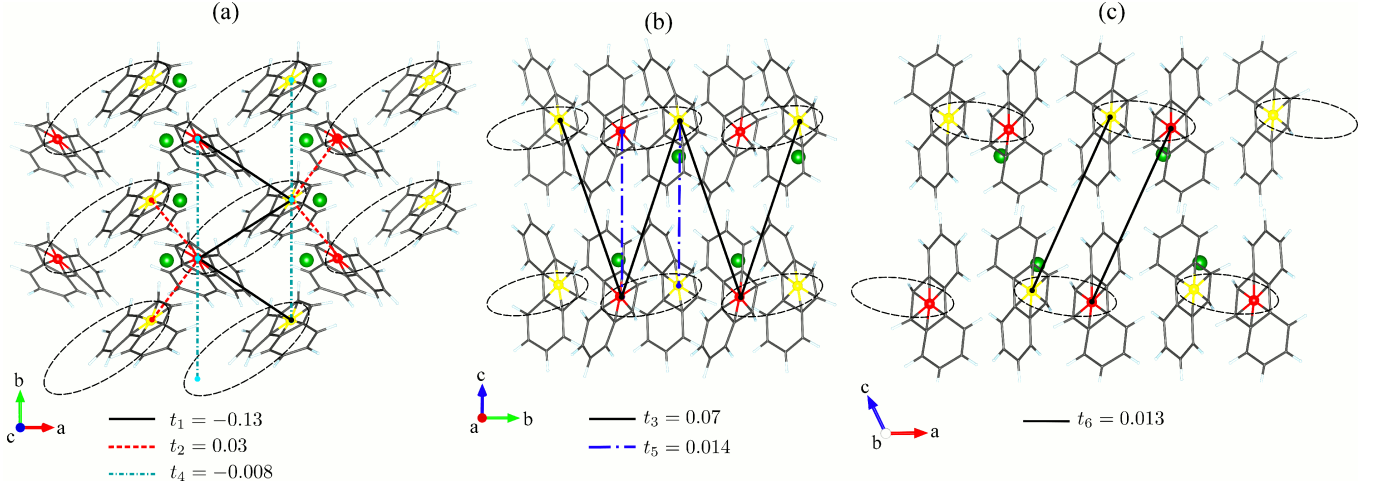
FIG. 5. (Color online) Wannier function hopping parameters in $a-b$, $b-c$, and $a-c$ planes. Red dot: PA molecule 1; yellow dot: PA molecule 2; green dot: La atom. The unit cell containing two PA molecules is encircled by dashed lines. The strongest hopping elements are drawn by heavy lines.

if $t_{\mathbf{k}}^{11} - t_{\mathbf{k}}^{22} = \Delta$ is the LUMO+1 orbital splitting of the two molecules in the unit cell, then $\tau_{\mathbf{k}}$ in Eq. (2) changes into

$$\tau_{\mathbf{k}} \to \sqrt{\Delta^2 + |t_{\mathbf{k}}^{12}|^2}, \qquad (4)$$

so that the degeneracy is lost at $\mathbf{k} \cdot \mathbf{b} = \pi$, where $|t_{\mathbf{k}}^{12}|^2 = 0$. Another possibility to remove the screw axis induced degeneracy is dimerization of PA molecules, even without inequivalence. Let us assume, for instance, that the hopping t_1 between two molecules in the same unit cell increases $t_1 \to t_1(1+\delta)$, while that between molecules on different unit cells diminishes $t_1 \to t_1(1-\delta)$. It follows that

$$t_{\mathbf{k}}^{12} \to t_{\mathbf{k}}^{12} + t_1 \delta \left(1 - e^{-i\mathbf{k} \cdot \mathbf{b}} \right), \qquad (5)$$

hence

$$\tau_{\mathbf{k}} \to \sqrt{4 t_1^2 \delta^2 \sin^2 \left(\frac{\mathbf{k} \cdot \mathbf{b}}{2} \right) + |t_{\mathbf{k}}^{12}|^2}, \qquad (6)$$

does not vanish anymore on the plane $\mathbf{k} \cdot \mathbf{b} = \pi$.

It is clear that if the energy splitting Δ or the dimerization δ exceed a threshold, then the two LUMO+1 derived bands cease to overlap and the band structure turns insulating, which is impossible if the two bands remains strictly degenerate on the plane $\mathbf{k} \cdot \mathbf{b} = \pi$. We finally note, as mentioned above, that an insulating state could also be realized by a sufficiently strong antiferromagnetic ordering, inducing a spin dependent splitting $\Delta_\uparrow = -\Delta_\downarrow$ between the LUMO+1 orbitals of the two molecules.

Thus the metallic state is highly fragile against perturbations or fluctuations that either tend to make the two molecules inequivalent, with or without magnetism, or else induce a dimerization pattern. If we aim at identifying processes that could mediate superconductivity, it

is a natural choice to focus on either structural (phonon) fluctuations, or on antiferromagnetic fluctuations of the above types, since they would most readily destabilize the metallic state. Although we cannot exclude that magnetic fluctuations could play the major role, we shall follow here a more conventional BCS approach and analyze qualitatively the electron-phonon coupling to modes that make the metallic state most unstable.

IV. DIMERIZING PHONON

We want to address and model here the simplest and most basic mechanism by which the metallic electronic states near the Fermi level are coupled to vibrations of the La-PA lattice. As an alternative to full fledge, system specific DFT electron phonon calculations which already exist ,[12] we wish to pursue here a simplified model of more generic use. We are guided by the physical consideration that the most important vibrations are all those that instantaneously break the symmetry induced degeneracy and open up a gap near the Fermi level. In that sense, the situation bears some analogy with that of MgB$_2$, where a frozen-in E$_{2g}$ vibration linearly splits the degeneracy of the σ band edge at the Γ point and near the Fermi level.[40]

In our $P2_1$ model structure, the degeneracy on the plane $\mathbf{k} \cdot \mathbf{b} = \pi$ can be removed by $\mathbf{q} = 0$ optical phonon, of either intramolecular or intermolecular character, inducing, respectively, an instantaneous energy splitting Δ or dimerization δ, as previously discussed. Although both phonons can be expected to be relevant in practice, as was found in electron phonon calculations of K$_3$ picene[37] we focus our attention on the intermolecular mode. The strongest intermolecular hopping is t_1 in the ab-plane. (see Fig. 5). A lattice vibration bringing closer the two molecules within each unit cell along the direc-
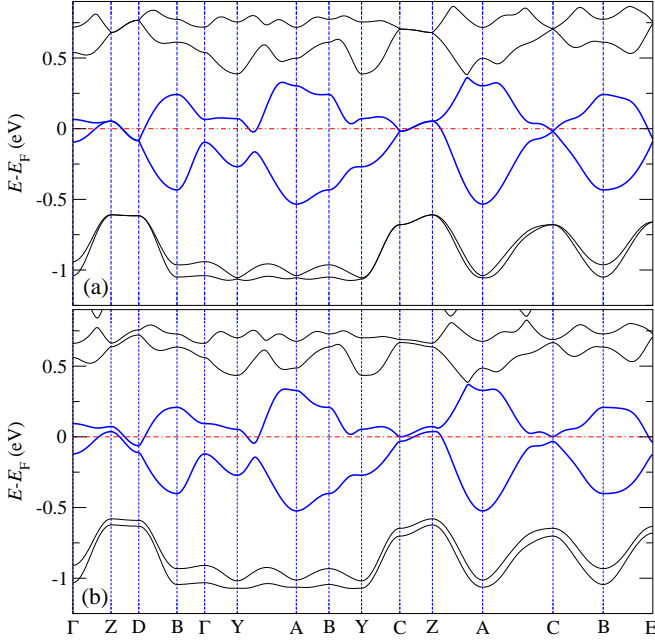
FIG. 6. (Color online) Band structure of metallic La-PA (structure 18) (a) before and (b) after a frozen-in dimerization distortion modulating the distance of molecules 1 and 2 by $\pm$ 0.08 Å in the ab plane, along the direction of hopping t_1 (see Fig. 5). The frozen phonon very effectively lifts the symmetry induced degeneracy at the Brillouin zone boundary opening up a gap at the Fermi level, see blue lines).

tion of hopping t_1 is therefore a reasonable first guess for a strongly coupled mode.

We thence consider a lattice periodic static distortion – a frozen phonon – corresponding to the above mentioned dimerization, where molecules 1 and 2 within each unit cell move toward each other in the ab-plane. We showed previously that this frozen phonon can destroy the zone boundary degeneracy, and open very effectively a band gap. To verify the magnitude of that effect we carried out DFT calculations where the initial metallic structure 18 was progressively "dimerized" in steps of 0.02 Å. Fig. 6 compares the band structure of original La-PA 18 with that where the 1-2-1 distances in the ab plane now alternate by $\pm$ 0.08 Å. As is seen, the gap indeed opens with great efficiency, whereas the rest of bands remain practically intact.

It is worth highlighting that the dimerizing distortion, although able to split the degeneracy on the $\mathbf{k} \cdot \mathbf{b} = \pi$ plane, nonetheless increases the total energy. In other words, the original undistorted $P2_1$ structure is stable towards a dimerization that leaves the two molecules within the unit cell equivalent, as well as towards a weak distortion that induces charge disproportionation between the two molecules, thus making them not equivalent. In fact, the $P2_1$ structure is found to be a stable local minimum, disconnected from the absolute minimum of $P1$ symmetry previously discussed.

A. Effective two-band model

We now include the dimerization mode in a model Hamiltonian for the LUMO+1 derived bands. The non-interacting tight-binding Hamiltonian is that of section III, i.e.
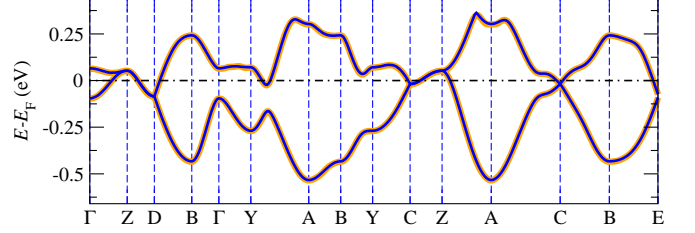

FIG. 7. (Color online) The two LUMO+1 derived bands used for modeling. The bold orange lines are Wannier parametrized bands, indistinguishable from the DFT results. Extracted hopping parameters are listed in Fig 5.

$$\mathcal{H}_0 = \sum_{\mathbf{k}\sigma} \left(c_{1\mathbf{k}\sigma}^\dagger, c_{2\mathbf{k}\sigma}^\dagger \right) \begin{pmatrix} t_\mathbf{k} & t_\mathbf{k}^{12} \\ t_\mathbf{k}^{12\,*} & t_\mathbf{k} \end{pmatrix} \begin{pmatrix} c_{1\mathbf{k}\sigma} \\ c_{2\mathbf{k}\sigma} \end{pmatrix}, \quad (7)$$

where $c_{1(2)\mathbf{k}\sigma}^\dagger$ creates an electron in LUMO+1 orbital (see Fig. 7) of molecule 1(2) with crystal momentum $\mathbf{k}$ and spin σ. We assume that each molecule can displace from its equilibrium position and such displacement affects primarily the hopping between molecule 1 and 2. Specifically, we shall consider the electron-phonon coupling of the classic "Fröhlich" type [41,42]

$$\mathcal{H}_{\text{el-ph}} = \sum_{\mathbf{R},\mathbf{R}_i} \sum_\sigma g_{|\mathbf{R}-\boldsymbol{\delta}|} \, t_\mathbf{R}^{12} \left(\mathbf{u}_{1\mathbf{R}_i+\mathbf{R}} - \mathbf{u}_{2\mathbf{R}_i} \right) \cdot \left(\mathbf{R} - \boldsymbol{\delta} \right)$$
$$\left(c_{1\mathbf{R}+\mathbf{R}_i\sigma}^\dagger c_{2\mathbf{R}_i\sigma} + H.c. \right), \quad (8)$$

where $\mathbf{u}_{1(2)\mathbf{R}}$ is the displacement of the molecule 1(2) in the unit cell with coordinate $\mathbf{R}$ and we have assumed that the variation of the hopping at linear order in the displacement,

$$\delta t_\mathbf{R}^{12} \simeq g_{|\mathbf{R}-\boldsymbol{\delta}|} \, t_\mathbf{R}^{12} \left(\mathbf{u}_{1\mathbf{R}_i+\mathbf{R}} - \mathbf{u}_{2\mathbf{R}_i} \right) \cdot \left(\mathbf{R} - \boldsymbol{\delta} \right),$$

is proportional to $t_\mathbf{R}^{12}$ at the equilibrium positions, with $\boldsymbol{\delta}$ the vector connecting the two molecules in the unit cell. We shall concentrate on displacement modes polarized along the b axis, i.e. $\mathbf{u}_{1(2)\mathbf{R}} = \left(u_{1(2)\mathbf{R}}^a, u_{1(2)\mathbf{R}}^b, u_{1(2)\mathbf{R}}^c \right) = \left(0, u_{1(2)\mathbf{R}}, 0 \right)$, which can induce a dimerization pattern able to turn the metal into an insulator. It follows that the Fourier transform of the electron-phonon coupling

$$\gamma_\mathbf{k} \equiv \sum_\mathbf{R} g_{|\mathbf{R}-\boldsymbol{\delta}|} \, t_\mathbf{R}^{12} \, e^{-i\mathbf{k}\cdot\mathbf{R}} \left(R^b - \delta^b \right) \propto \left(1 - e^{-i\mathbf{k}\cdot\mathbf{b}} \right), \quad (9)$$

hence finite on the degeneracy plane $\mathbf{k} \cdot \mathbf{b} = \pi$. The Fourier transform of the electron-phonon Hamiltonian

(8) thus reads

$$\mathcal{H}_{\text{el-ph}} = \sum_{\mathbf{k},\mathbf{q},\sigma} \left(u_{1-\mathbf{q}}\,\gamma_{\mathbf{k}+\mathbf{q}} - u_{2-\mathbf{q}}\,\gamma_{\mathbf{k}} \right) c^{\dagger}_{1\mathbf{k}\sigma} c_{2\mathbf{k}+\mathbf{q}\sigma}$$
$$+ \left(u_{1-\mathbf{q}}\,\gamma_{-\mathbf{k}} - u_{2-\mathbf{q}}\,\gamma_{-\mathbf{k}-\mathbf{q}} \right) c^{\dagger}_{2\mathbf{k}\sigma} c_{1\mathbf{k}+\mathbf{q}\sigma}. \quad (10)$$

An out-of-phase displacement of the two molecules is characterized by $u_{1\mathbf{q}} = x_{\mathbf{q}}$ and $u_{2\mathbf{q}} = -\mathrm{e}^{-i\mathbf{q}\cdot\mathbf{b}/2}\,x_{\mathbf{q}}$, with $x_{\mathbf{q}}$ the optical eigenmode, so that

$$\mathcal{H}_{\text{el-ph}} = \sum_{\mathbf{k},\mathbf{q},\sigma} x_{-\mathbf{q}}\Big(\gamma_{\mathbf{k}+\mathbf{q}} + \mathrm{e}^{i\mathbf{q}\cdot\mathbf{b}/2}\,\gamma_{\mathbf{k}} \Big) c^{\dagger}_{1\mathbf{k}\sigma} c_{2\mathbf{k}+\mathbf{q}\sigma}$$
$$+ x_{-\mathbf{q}}\Big(\gamma_{-\mathbf{k}} + \mathrm{e}^{i\mathbf{q}\cdot\mathbf{b}/2}\,\gamma_{-\mathbf{k}-\mathbf{q}} \Big) c^{\dagger}_{2\mathbf{k}\sigma} c_{1\mathbf{k}+\mathbf{q}\sigma}. \quad (11)$$

In addition, we must include the phonon Hamiltonian

$$\mathcal{H}_{\text{ph}} = \sum_{\mathbf{q}} \frac{\omega_{\mathbf{q}}}{2} \left(p_{\mathbf{q}} p_{-\mathbf{q}} + x_{\mathbf{q}} x_{-\mathbf{q}} \right), \quad (12)$$

with $\left[x_{\mathbf{q}}, p_{-\mathbf{q}'} \right] = i\delta_{\mathbf{q}\mathbf{q}'}$.

The final ingredient we need to include is the electron-electron interaction. The simplest term that accounts for the suppression of charge fluctuations in such a narrow-band molecular conductor is a Hubbard repulsion

$$\mathcal{H}_{\text{U}} = U \sum_{\mathbf{R}} n_{1\mathbf{R}\uparrow} n_{1\mathbf{R}\downarrow} + n_{2\mathbf{R}\uparrow} n_{2\mathbf{R}\downarrow}. \quad (13)$$

Numerical values for U have been given for a number of PAHs including phenanthrene by Nomura et al.[38] They were generally found to be large, in fact quite similar to the electron bandwidths. In reality, since those values refer to a 4-band model that includes also LUMO besides LUMO+1, the corresponding estimates for a 2-band model aiming at describing just LUMO+1 must be smaller, since they already account for the LUMO screening of the effective U among LUMO+1 electrons.

In summary, our proposed Hamiltonian is a "Hubbard-Fröhlich" one

$$\mathcal{H} = \mathcal{H}_0 + \mathcal{H}_{\text{ph}} + \mathcal{H}_{\text{el-ph}} + \mathcal{H}_{\text{U}}, \quad (14)$$

It does in our view include the main ingredients present in a generic $P2_1$ metallic phase – La-PA, or in fact any other three-electron-doped PAH crystal with that kind of high symmetry.

V. DISCUSSION AND CONCLUSIONS

We have conducted a theoretical study of La-phenanthrene, here adopetd as a generic model of electron-doped PAHs, where a number of superconducting phases have been experimentally proposed. Exploring by ab initio calculations a large variety of bimolecular structures, we found that the lowest energy state of La-PA is not metallic as expected, but is a band insulator resulting from a symmetry-lowering disproportionation of the two PA molecules. In that phase of La-PA an optical band gap of 0.7 eV or larger should be observable in near infrared, along with vibrational signatures of the disproportionation between the two molecules.

At higher total energy we also found and characterized high symmetry metallic phases, whose electronic structures resemble those proposed for alkali doped picene. Although in La-PA this metallic phase could only exist as a metastable state, we studied it in detail with the scope of extracting a generic two-band model containing interesting elements that could determine and control the superconductivity of more general electron-doped PAHs, where many elements are similar. The two bands are derived from LUMO+1 molecular orbitals and were extracted from a tight binding fit of the La-PA ab initio bands near the Fermi level. An important phonon with a standard Fröhlich coupling to the electrons in these bands was identified as a dimerizing intermolecular vibration, which acts by breaking a symmetry-induced band degeneracy near Fermi. The strong electron-electron repulsion U typical of PAH ions constitutes the third important element of that model. We conclude proposing this overall two band "Hubbard-Fröhlich" model for further studies of superconductivity in these systems. While the superconducting solution of this model and its properties will be the subject of subsequent work, we underline here that it should in principle be applicable, given its symmetry motivated, highly schematic form, to a broad family of electron-doped PAHs, and not just to La-PA, whose metallic phase, predicted to be metastable at best, is still waiting to be properly identified and characterized.

[1] R. Mitsuhashi, Y. Suzuki, Y. Yamanari, H. Mitamura, T. Kambe, N. Ikeda, H. Okamoto, A. Fujiwara, M. Yamaji, N. Kawasaki, Y. Maniwa, and Y. and, Nature **464**, 76 (2010).

[2] Y. Kubozono, H. Mitamura, X. Lee, X. He, Y. Yamanari, Y. Takahashi, Y. Suzuki, Y. Kaji, R. Eguchi, K. Akaike, T. Kambe, H. Okamoto, A. Fujiwara, T. Kato, T. Kosugi, and H. Aoki, Phys. Chem. Chem. Phys. **13**, 16476 (2011).

[3] T. Kato, T. Kambe, and Y. Kubozono, Phys. Rev. Lett. **107**, 077001 (2011).

[4] M. Xue, T. Cao, D. Wang, Y. Wu, H. Yang, X. Dong, J. He, F. Li, and G. F. Chen, Sci. Rep. **2**, 389 (2012).

[5] X. Wang, R. Liu, Z. Gui, Y. Xie, Y. Yan, J. Ying, X. Luo, and X. Chen, Nature Commun. **2**, 507 (2011).

[6] X. F. Wang, Y. J. Yan, Z. Gui, R. H. Liu, J. J. Ying, X. G. Luo, and X. H. Chen, Phys. Rev. B **84**, 214523 (2011).

[7] X. F. Wang, X. G. Luo, J. J. Ying, Z. J. Xiang, S. L. Zhang, R. R. Zhang, Y. H. Zhang, Y. J. Yan, A. F. Wang, P. Cheng, G. J. Ye, and X. H. Chen, J. Phys. Condens. Matter **24**, 345701 (2012).

[8] B. Mahns, F. Roth, and M. Knupfer, J. Chem. Phys. **136**, 134503 (2012).

[9] M. Caputo, G. D. Santo, P. Parisse, L. Petaccia, L. Floreano, A. Verdini, M. Panighel, C. Struzzi, B. Taleatu, C. Lal, , and A. Goldoni, J. Phys. Chem. C **116**, 19902 (2012).

[10] A. Subedi and L. Boeri, Phys. Rev. B **84**, 020508 (2011).

[11] G. Giovannetti and M. Capone, Phys. Rev. B **83**, 134508 (2011).

[12] M. Casula, M. Calandra, G. Profeta, and F. Mauri, Phys. Rev. Lett. **107**, 137006 (2011).

[13] T. Kosugi, T. Miyake, S. Ishibashi, R. Arita, and H. Aoki, Phys. Rev. B **84**, 214506 (2011).

[14] P. L. de Andres, A. Guijarro, and J. A. Vergés, Phys. Rev. B **84**, 144501 (2011).

[15] T. Kosugi, T. Miyake, S. Ishibashi, R. Arita, and H. Aoki, J. Phys. Soc. Jpn. **78**, 113704 (2009).

[16] Z. Huang, C. Zhang, and H.-Q. Lin, Sci. Rep. **2**, 992 (2012).

[17] A. F. Hebard, M. J. Rosseinsky, R. C. Haddon, D. W. Murphy, S. H. Glarum, T. T. M. Palstra, A. P. Ramirez, and A. R. Kortan, Nature **350**, 600 (1991).

[18] M. Capone, M. Fabrizio, C. Castellani, and E. Tosatti, Science **296**, 2364 (2002).

[19] A. Y. Ganin, Y. Takabayashi, Y. Z. Khimyak, S. Margadonna, A. Tamai, M. J. Rosseinsky, and K. Prassides, Nature Materials **7**, 367 (2008).

[20] A. Y. Ganin, Y. Takabayashi, P. Jegli, D. Aron, A. Potonik, P. J. Baker, Y. Ohishi, M. T. McDonald, M. D. Tzirakis, A. McLennan, G. R. Darling, M. Takata, M. J. Rosseinsky, and K. Prassides, Nature **466**, 221 (2010).

[21] M. Capone, M. Fabrizio, C. Castellani, and E. Tosatti, Rev. Mod. Phys. **81**, 943 (2009).

[22] P. G. et al, J. Phys. Condens. Matter **21**, 395502 (2009).

[23] J. P. Perdew, K. Burke, and M. Ernzerhof, Phys. Rev. Lett. **78**, 1396 (1997).

[24] D. Vanderbilt, Phys. Rev. B **41**, 7892 (1990).

[25] J. Trotter, Acta Cryst. **16**, 605 (1963).

[26] M. Dion, H. Rydberg, E. Schröder, D. C. Langreth, and B. I. Lundqvist, Phys. Rev. Lett. **92**, 246401 (2004).

[27] K. Lee, E. D. Murray, L. Kong, B. I. Lundqvist, and D. C. Langreth, Phys. Rev. B **82**, 081101 (2010).

[28] S. Grimme, J. Comput. Chem. **25**, 1463 (2004).

[29] S. Grimme, J. Comput. Chem. **27**, 1787 (2006).

[30] T. Thonhauser, V. R. Cooper, S. Li, A. Puzder, P. Hyldgaard, and D. C. Langreth, Phys. Rev. B **76**, 125112 (2007).

[31] G. Román-Pérez and J. M. Soler, Phys. Rev. Lett. **103**, 096102 (2009).

[32] R. Sabatini, E. Kücükbenli, B.Kolb, T. Thonhauser, and S. de Gironcoli, J. Phys. Condens. Matter **24**, 424209 (2012).

[33] We thank A. Laio for this suggestion.

[34] We are grateful to Prof. R. Martonak for his help with these simulations.

[35] V. Heine, Group Theory in Quantum Mechanics (Pergamon Press, London, 1960).

[36] F. Bassani and G. P. Parravicin, Electron States and Optical Transitions in Solids (Pergamon Press, London, 1975).

[37] M. Casula, M. Calandra, and F. Mauri, Phys. Rev. B **86**, 075445 (2012).

[38] Y. Nomura, K. Nakamura, and R. Arita, Phys. Rev. B **85**, 155452 (2012).

[39] A. A. Mostofi, J. R. Yates, Y.-S. Lee, I. Souzab, D. Vanderbiltd, and N. Marzari, Comput. Phys. Commun. **178**, 685 (2008).

[40] A. Shukla, M. Calandra, M. d'Astuto, M. Lazzeri, F. Mauri, C. Bellin, M. Krisch, J. Karpinski, S. M. Kazakov, J. Jun, D. Daghero, and K. Parlinski, Phys. Rev. Lett. **90**, 095506 (2003).

[41] H. Fröhlich, Phys. Rev. **79**, 845 (1950).

[42] H. Fröhlich, Proc. Roy. Soc. London **215**, 291 (1952).